Title

Merits of Combination Cortical, Subcortical, and Cerebellar Injections for the Treatment of Niemann-Pick Disease Type A

Journal

Molecular Therapy, 20(10)

ISSN

1525-0016

Authors

Bu, Jie
Ashe, Karen M
Bringas, John
et al.

Publication Date

2012-10-01

DOI

10.1038/mt.2012.118

Peer reviewed

Merits of Combination Cortical, Subcortical, and Cerebellar Injections for the Treatment of Niemann-Pick Disease Type A

Jie Bu[1], Karen M Ashe[1], John Bringas[2], John Marshall[1], James C Dodge[1], Mario A Cabrera-Salazar[1], John Forsayeth[2], Edward H Schuchman[3], Krystof S Bankiewicz[2], Seng H Cheng[1], Lamya S. Shihabuddin[1] and Marco A Passini[1]

[1]Rare Diseases Division, Genzyme Corporation, Framingham, Massachusetts, USA; [2]Department of Neurosurgery, University of California, San Francisco, California, USA; [3]Department of Genetics and Genomic Sciences, Mount Sinai School of Medicine, New York, New York, USA

Niemann-Pick disease Type A (NPA) is a neuronopathic lysosomal storage disease (LSD) caused by the loss of acid sphingomyelinase (ASM). The goals of the current study are to ascertain the levels of human ASM that are efficacious in ASM knockout (ASMKO) mice, and determine whether these levels can be attained in non-human primates (NHPs) using a multiple parenchymal injection strategy. Intracranial injections of different doses of AAV1-hASM in ASMKO mice demonstrated that only a small amount of enzyme (<0.5 mg hASM/g tissue) was sufficient to increase survival, and that increasing the amount of hASM did not enhance this survival benefit until a new threshold level of >10 mg hASM/g tissue was reached. In monkeys, injection of 12 tracts of AAV1-hASM resulted in efficacious levels of enzyme in broad regions of the brain that was aided, in part, by axonal transport of adeno-associated virus (AAV) and movement through the perivascular space. This study demonstrates that a combination cortical, subcortical, and cerebellar injection protocol could provide therapeutic levels of hASM to regions of the NHP brain that are highly affected in NPA patients. The information from this study might help design new AAV-mediated enzyme replacement protocols for NPA and other neuronopathic LSDs in future clinical trials.

Received 22 February 2012; accepted 13 May 2012; advance online publication 24 July 2012. doi:10.1038/mt.2012.118

INTRODUCTION

Adeno-associated virus (AAV)-mediated gene therapy is an emerging technology for potentially treating a variety of neurologic diseases. A family of disorders that could benefit from this technology is the neuronopathic lysosomal storage diseases (LSDs) that collectively present with an incidence of 1:8,000 live births.[1] LSDs are monogenic disorders caused by mutations in genes encoding lysosomal enzymes that are responsible for metabolizing a broad spectrum of cellular substrates. A deficiency in one or more of these enzymatic activities invariably result in the accumulation of undigested substrates in the lysosomes of cells. Approximately 70% of LSDs have brain and spinal cord involvement due to the accumulation of storage materials in neurons and glia, which leads to neurodegeneration and death typically in childhood.[2,3] Several laboratories have independently shown that delivering the normal version of the affected gene into the central nervous system (CNS) of animal models of LSDs is corrective, thereby demonstrating the utility of gene therapy for treating this group of disorders.[2,3] However, because the brain size of mice are small compared to humans, studies in mouse models of LSDs only serve as proof-of-concept that gene therapy is efficacious. Further studies are required to address the challenges associated with global delivery of a viral vector to the CNS in children.

A challenge facing the clinical application of gene therapy for neuronopathic LSDs is the development of a facile and practical method that effects widespread gene delivery to the CNS. The blood–brain barrier and the likelihood of pre-existing immunity to the viral capsid proteins presents significant challenges to systemic delivery of AAV as a clinically relevant approach for neurodegenerative diseases.[4] Direct intracranial injection of the recombinant AAV vectors can potentially circumvent these issues. Indeed, this route of delivery is currently in clinical testing for Parkinson's disease, Alzheimer's disease, Canavan disease, and late infantile neuronal ceroid lipofuscinosis (LINCL).[5–14] A major advantage of treating neuronopathic LSDs is that many of the lysosomal enzymes are soluble hydrolases that are secreted into the extracellular matrix which are then taken-up by neighboring cells, a process that is referred to as cross-correction. This bystander property means that not every neural cell needs to be transduced by the viral vector to be corrected.[2,3] Thus, targeting regions in the non-human primate (NHP) brain that promote widespread distribution of the AAV vector and enzyme from the sites of injections might increase the probability of success in the clinic.

Niemann-Pick disease Type A (NPA) is a neuronopathic LSD caused by the loss of acid sphingomyelinase (ASM) activity and subsequent accumulation of sphingomyelin (SPH) in the CNS and viscera of affected children.[15] An ASM knockout (ASMKO) mouse model that recapitulates several pathophysiological features that are characteristic of NPA patients has been generated.[16]

Correspondence: *Marco A Passini, 49 New York Avenue, Genzyme Corporation, Framingham, Massachusetts 01701-9322, USA. E-mail: marco.passini@genzyme.com*

We have previously shown that CNS-directed AAV-hASM therapy can ameliorate storage pathology and improve the motor function and survival of ASMKO mice.[17–19] However, these studies did not address the minimum amount of ASM levels required for efficacy, which is an important consideration when interpreting translational biodistribution studies in the NHP. Recently, Salegio *et al.* (2010) showed AAV-mediated expression of hASM in the NHP brain following administration of the viral vector into the pons.[20] Although the reported vector distribution from pontine injections was encouraging, questions remain about the translatability of this site of injection because of the potential detrimental risk associated with an accidental hemorrhaging of the pons. Thus, the work by Salegio *et al.* (2010) only validated that AAV could be used to deliver ASM to the NHP using magnetic resonance imaging (MRI) guidance, but did not necessarily provide a translatable protocol for the clinic.

In the current study, we investigated an injection protocol that simultaneously targeted multiple brain structures that have been shown in previous clinical studies to tolerate injections of gene therapy vectors. We hypothesized that widespread enzyme expression in a large brain could be achieved by combining cortical and subcortical sites (based on experiences from previous trials) into one injection protocol. Furthermore, we tested whether the deep cerebellar nucleus (DCN) shown previously to support widespread enzyme distribution in ASMKO mice,[18] was equally judicious in the NHP for ASM expression in the brain stem. Finally, before initiating the NHP study, we performed a dose-response study in ASMKO mice to identify the minimum hASM levels required for efficacy.

RESULTS

Efficacy of intracranial administration of AAV1-hASM into ASMKO mice

Different doses of an AAV serotype-1 vector encoding human ASM (AAV1-hASM) was stereotactically injected into the ASMKO mouse brain to determine the levels of hASM necessary for efficacy. AAV1 was chosen because this serotype has been shown to provide better spread and higher levels of transgene expression compared to AAV2 in the murine, feline, and NHP brains.[18,21–29] Multiple brain regions of ASMKO mice at the presymptomatic age of 8 weeks were injected with AAV1-hASM for a final dose of 1.2×10^{11}, 4.0×10^{10}, 1.2×10^{10}, or 4.0×10^{9} genome copies (gc) per mouse. The targeted brain regions were chosen because they are highly affected in ASMKO mice and in NPA patients. Treated and untreated ASMKO mice were killed when they became moribund, and the left hemisphere from each brain was processed for hASM levels and the right hemisphere for SPH storage ($n = 6$ per group).

Enzyme-linked immunosorbent assay (ELISA) analysis of brain homogenates from the left hemisphere showed a dose-dependent increase in hASM levels with mice receiving the highest dose (1.2×10^{11} gc) exhibiting the greatest levels of hASM (9.6–13.6 ng hASM/mg tissue) (**Figure 1**, **Table 1**). Abundant amounts of hASM were also detected in the brains of mice treated with the two intermediate doses (4.0×10^{10} and 1.2×10^{10} gc) albeit at lower levels (1.9–7.4 ng hASM/mg tissue) than in animals that received the highest dose. In contrast, hASM levels in mice administered the lowest dose (4.0×10^{9} gc) were barely detectable in this assay (0.1–0.4 ng hASM/mg tissue). A commensurate

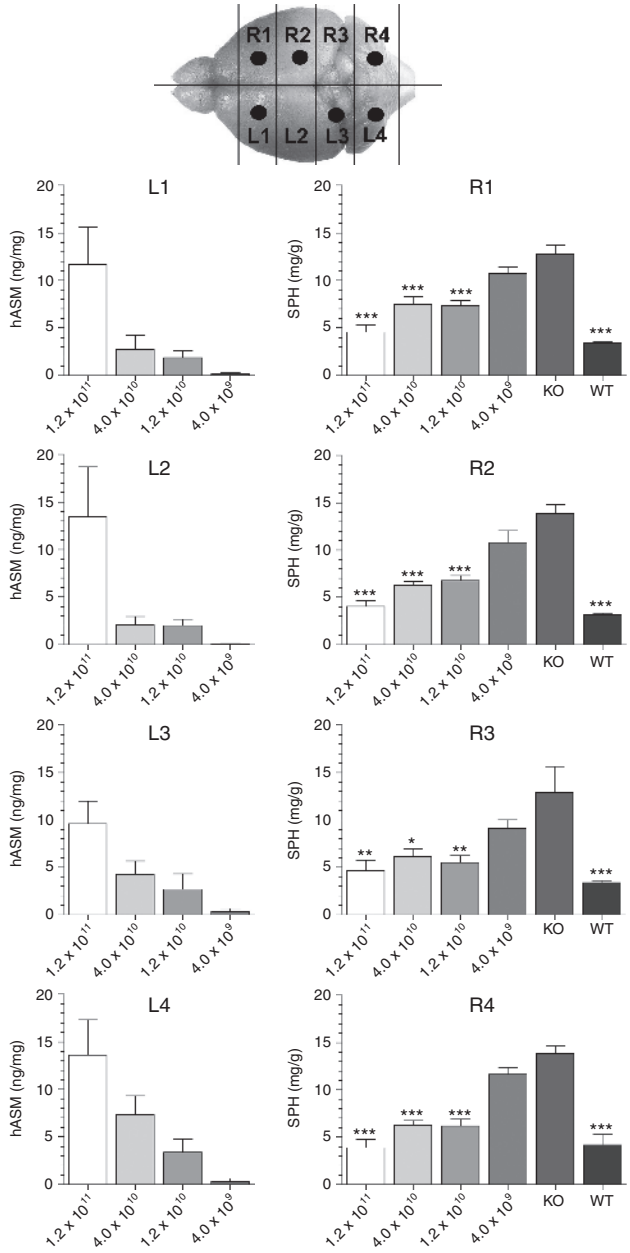

Figure 1 Levels of hASM enzyme and SPH lipid following intracranial injection of different doses of AAV1-hASM in ASMKO mice. Before homogenization, the right and left hemispheres were separated and further divided into four coronal slabs. Brain slabs that contained an injection site were marked with a black circle in the above diagram. ELISA assays (left column) showed a dose-dependent increase in hASM levels throughout the brain. SPH assays (right column) showed a significant reduction in SPH levels in all the brain slabs following treatment with the highest (1.2×10^{11} gc) and both intermediate (4×10^{10}, 1×10^{10} gc) doses compared to untreated ASMKO. Furthermore, mice administered the highest dose was the only group that contained SPH levels that was not statistically different than WT mice in all the brain slabs ($P > 0.05$), indicating that global reduction of SPH to near normal levels was achieved with 1.2×10^{11} gc of AAV1-hASM. Although the lowest dose (4×10^{9} gc) provided a decrease in brain storage, the SPH levels were not significantly different from untreated ASMKO mice ($P > 0.05$). The statistical analysis used was a one-way variance (ANOVA) and Bonferroni multiple post hoc comparison (*$P < 0.05$; ** $P < 0.01$; ***$P < 0.001$), $n = 6$ for each group. AAV, adeno-associated virus; ANOVA, analysis of variance; ASMKO, acid sphingomyelinase knockout; ELISA, enzyme-linked immunosorbent assay; gc, genome copies; SPH, sphingomyelin; WT, wild-type.

Table 1 Correlation of vector dose with hASM levels, SPH storage, and median survival in ASMKO mice

Mouse	AAV1-hASM dose (gc)	Mean hASM levels per brain slab (ng ASM/ mg tissue)	Mean SPH levels per brain slab (mg SPH/ g tissue)	Median survival (weeks)
ASMKO	0 (untreated control)	<0.08 (assay background)	12.8–13.9	34.0
ASMKO	4.0×10^9	0.1–0.4	9.1–11.7	41.0
ASMKO	1.2×10^{10}	1.9–3.4	5.5–6.8	42.0
ASMKO	4.0×10^{10}	2.1–7.4	6.2–7.5	41.5
ASMKO	1.2×10^{11}	9.6–13.6	3.9–4.6	52.0
Wild-type	0 (untreated control)	ND[a]	3.1–4.2	>100[b]

Abbreviations: AAV, adeno-associated virus; ASMKO, acid sphingomyelinase knockout; gc, genome copies; ND, not determined; SPH, sphingomyelin.
Shown are the average (mean) ranges of hASM and SPH levels detected in the individual brain slabs, and the resulting longevity in ASMKO mice.
[a]The values of hASM levels were not determined in wild-type mice. However, we anticipate the values to be at the assay background (<0.08 ng/mg) because the anti-hASM antibody does not cross-react with endogenous mouse ASM. [b]Untreated wild-type mice in our facility can live up to 2.0–2.5 years.

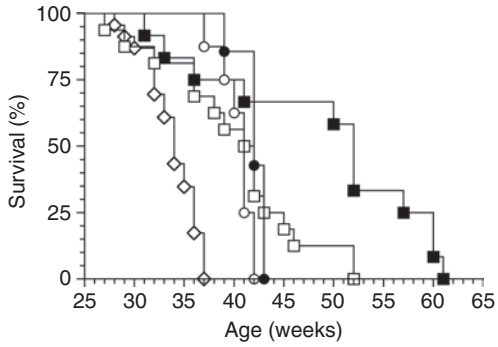

Figure 2 All doses of AAV1-hASM improved the median survival of ASMKO mice. Shown is a Kaplan–Meier survival curve of untreated ASMKO mice ($n = 23$, open diamonds), and treated ASMKO mice that received a dose of 1.2×10^{11} ($n = 12$, closed squares), 4.0×10^{10} ($n = 16$, open squares), 1.2×10^{10} ($n = 7$, closed circles), and 4.0×10^9 ($n = 8$, open circles) genome copies per mouse. All treated ASMKO mice showed a significant improvement in median survival compared to ASMKO controls ($P < 0.0001$). AAV, adeno-associated virus; ASMKO, acid sphingomyelinase knockout.

dose-dependent decrease in SPH levels was also observed in the brains of ASMKO mice (**Figure 1**, **Table 1**). Treatment with the highest viral dose resulted in a significant reduction in SPH (3.9–4.6 mg SPH/g tissue) to levels that approached wild-type levels ($P < 0.001$). Significant reductions in SPH (5.5–7.5 mg SPH/g tissue) were also attained with the two intermediate doses ($P < 0.001$). Consistent with the low levels of hASM, ASMKO mice administered the lowest dose provided the least reduction in SPH storage (to 9.1–11.7 mg SPH/g tissue, compared to 12.8–13.9 mg SPH/g tissue in untreated ASMKO controls, $P > 0.05$). Although the range of ages at the time of killing was not large (see Materials and Methods), some of the variability in the levels of SPH might have been due to the animals being not fully age-matched.

All doses of AAV1-hASM provided a significant survival benefit in ASMKO mice (**Figure 2**, **Table 1**). ASMKO mice treated with the highest dose exhibited a median survival of 52 weeks compared to 34 weeks in untreated ASMKO controls (53% increase in median survival, $P < 0.0001$). Furthermore, ASMKO mice treated with 4×10^{10}, 1×10^{10}, and 4×10^9 gc produced similar median survivals of 41.5 (22% increase, $P < 0.0001$), 42 (24%, $P < 0.0001$), and 41 (20%, $P < 0.0001$) weeks, respectively. Interestingly, the lowest dose group (4×10^9 gc) demonstrated that significant longevity could be induced in mice just by decreasing a small amount of SPH storage. This observation supports the prevailing notion that only a small amount of lysosomal enzyme is sufficient to provide efficacy in affected cells.[1–3] Although the cohort treated with the highest dose (1.2×10^{11} gc/mouse) reduced SPH storage in the brain to near normal levels, these mice eventually succumbed to the visceral disease. We previously showed that correction of both the visceral and brain components of the disease is a necessary prerequisite for the complete rescue of ASMKO mice.[19]

AAV1-hASM gene transfer to the CNS of cynomolgus monkeys

A large animal model for NPA does not exist. However, the size and anatomy of the cynomolgus brain is an appropriate animal model to address the challenges of widespread CNS delivery. Thus, to determine the feasibility of achieving clinically relevant widespread hASM expression in a large brain, the same lot of AAV1-hASM used in the ASMKO dose-response study was injected into different regions of the cynomolgus brain ($n = 2$). Two year old juvenile monkeys were chosen because they approximate the physiological age of young children that would receive therapeutic intervention. Each monkey received convection-enhanced injections into 6 sites per hemisphere for a total of 12 sites per brain. The motor cortex, occipital cortex, striatum, and thalamus each received 2.5×10^{11} gc (50 µl each), and the hippocampus and cerebellum each received 1.5×10^{11} gc (30 µl each). Thus each hemisphere received 1.3×10^{12} gc (260 µl) for a total of 2.6×10^{12} gc (520 µl) of AAV1-hASM per brain. These brain regions were chosen because they are highly affected in NPA patients, and injections into many of these structures were well tolerated in other gene therapy clinical trials.[5–14] As a control, a third monkey received 520 µl of saline per brain using the same injection strategy. Monkeys were killed 5 weeks after injection; the right hemisphere was analyzed by immunohistochemistry to determine the hASM expression pattern, and the left hemisphere was analyzed by ELISA to determine the levels of total ASM (endogenous and vector-derived).

In the right hemisphere, hASM expression was observed in many regions of the cynomolgus brain. The injected cerebral cortex showed a stark partitioning of hASM mRNA and protein to mostly gray matter in both the motor and occipital lobes (**Figure 3a–e**). In the subcortical regions, large areas of the injected striatum and thalamus showed robust hASM expression (**Figure 4a–c**). Robust hASM expression was also observed in the CA1–CA3 pyramidal cell layers and dentate gyrus of the injected hippocampus (**Figure 4d–f**). Furthermore, hASM mRNA and protein was detected in pyramidal cell layers II and III of the entorhinal cortex (**Figure 4g–i**). These superficial layers of the entorhinal cortex send extensive axonal projections to the hippocampus, demonstrating that uninjected regions of the brain can become targeted by axonal transport of AAV. In the cerebellum, robust expression was observed in the injected DCN (**Figure 5a,b**). Furthermore,

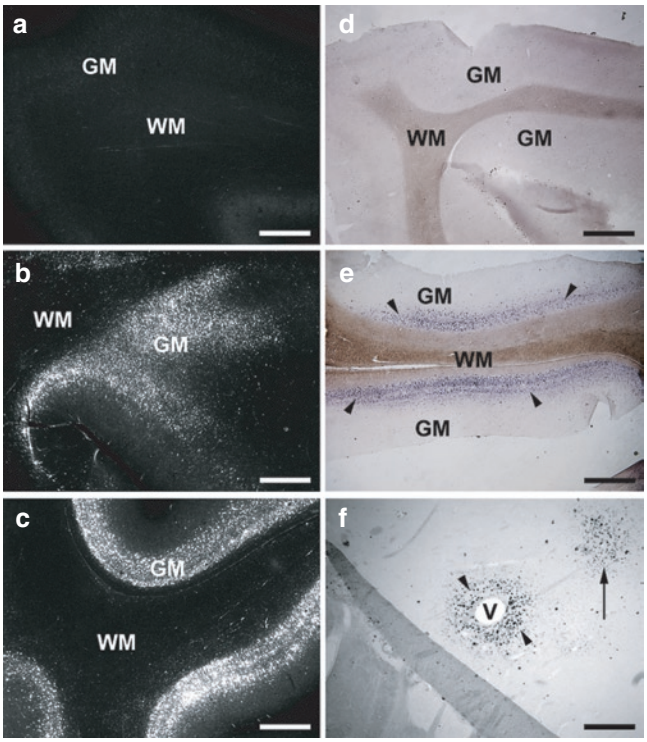

Figure 3 Cortical injections of AAV1-hASM in NHPs. (**a**–**c**) Immunohistochemistry and (**d**–**f**) *in situ* hybridization of the (**a**,**b**) motor cortex and the (**c**–**e**) occipital cortex in (**a**,**d**) saline-treated and (**b**,**c**,**e**,**f**) AAV1-hASM–treated monkeys. The arrowheads in **e** point to a band of *in situ* hybridization-positive cells in the gray matter (purple color) immediately adjacent to the white matter. *In situ* hybridization in a region of the brain outside the injection sites showed hASM mRNA expression surrounding blood vessels (**f**, arrowheads). In some cases, a similar pattern of gene expression could also be observed outside the plane of the blood vessel (arrow). GM, gray matter; V, blood vessel; WM, white matter. Bars: 1.0 mm (in **a**–**c**); 2.0 mm (in **d**,**e**); 0.5 mm (in **f**). AAV, adeno-associated virus; NHP, non-human primate.

hASM mRNA and protein was observed in Purkinje cells of the uninjected cerebellar cortex (Figure 5c,d), and in projection neurons of the uninjected medulla oblongata (Figure 5c–h) and spinal cord (Figure 5i,j). This pattern of hASM expression is consistent with axonal transport of AAV from the DCN injection site. Finally, a cross-section of a large blood vessel in the brain revealed *in situ* hybridization-positive signals surrounding the blood vessel (Figure 3f). These "satellite" transduction pattern were intermittingly dispersed in both cortical and subcortical regions, suggesting that distal and remote regions of the brain can become targeted *via* movement of the AAV vector through the perivascular space.[30]

ELISA analysis of the left hemisphere showed an increase in total ASM levels after AAV1-hASM treatment (Figure 6). Brain slabs with total ASM levels that were at least 2 SDs above the baseline mean of the saline-treated monkey were considered statistically significant (see Materials and Methods). Brain slabs that contained an injection site showed a significant increase in total ASM ranging from 51.2–202.9 ng ASM/mg tissue (monkey 1) and 43.2–161.4 ng ASM/mg tissue (monkey 2), compared to 23.745 ± 6.583 ng ASM/mg tissue (mean ± SD) in the corresponding regions of the saline-treated control animal. Significant elevated levels of total ASM outside the injection sites were also detected in the cerebral cortex ranging from 38.8–75.5 ng ASM/mg tissue (monkey 1) and 43.2–59.3 ng ASM/mg tissue (monkey 2), and in the subcortical regions ranging from 57.7 ng ASM/mg tissue (monkey 1) and 51.1–70.7 ng ASM/mg tissue (monkey 2). Furthermore, the medulla oblongata of monkey 2 (24.0 ng ASM/mg tissue) and the spinal cord of monkey 1 (25.4 ng ASM/mg tissue) contained an increase in total ASM levels compared to saline treatment (12.340 ± 4.904 ng ASM/mg tissue (mean ± SD)). Although we had clear evidence of vector-derived expression in the Purkinje cell layer (Figure 5c,d), we did not detect a significant increase in total ASM in the cerebellar cortex of both AAV1-treated monkeys. This result might have been due to the fact that cerebellar granule cells, which do not send axonal projections to the DCN, account for the vast majority of neurons in the cerebellar cortex thus masking the hASM levels in homogenized tissue. Furthermore, the lack of a significant increase in total ASM in the cerebral cortex between the motor and occipital lobes suggests that additional cortical deposits, or utilization of axonal transport *via* the cortico-thalamic circuitry with additional thalamic deposits,[31] might be needed to achieve a more comprehensive enzyme distribution in the cerebral cortex.

DISCUSSION

In the current study, we first investigated the relationship between hASM expression levels, SPH storage, and median survival in ASMKO mice. Intracranial injections with the highest dose of AAV1-hASM in ASMKO mice resulted in >10 ng hASM/mg tissue throughout the brain, and a concomitant decrease in SPH storage to near normal levels and a 50% increase in median survival. Administration of the lowest and two intermediate doses of AAV1-hASM produced correspondingly lower levels of hASM and lesser reductions in SPH levels. Although the resulting levels of enzyme and storage were different between the low and two intermediate doses, they all produced 20–24% increases in median survival. Hence, the linear relationship between hASM and SPH did not translate to a linear improvement in survival. As the mice treated with the highest dose of virus afforded near complete clearance of SPH, the data suggests that residual SPH confer some measure of cellular toxicity, and that maximal removal of the offending substrate from the brain was necessary for the greatest improvement in survival. Future efficacy studies in ASMKO mice would benefit from the inclusion of an empty vector control group (*i.e.*, AAV1-Null).

We next examined the feasibility of achieving widespread distribution of hASM in the NHP through injection of multiple brain structures with convection-enhanced delivery. We demonstrate that a combination of cortical, subcortical, and cerebellar injections is an effective method for effecting widespread AAV-mediated enzyme expression in the NHP brain including regions that are highly affected in NPA. The highest levels of total ASM were found in the brain slabs that contained an injection site, which clearly exceeded the threshold level (>10 ASM ng/mg tissue) required for the longest survival in CNS-treated ASMKO mice. However, future toxicity studies that include an empty vector control group will be required to address the safety of producing supraphysiologic levels of hASM in focal regions (injection sites)

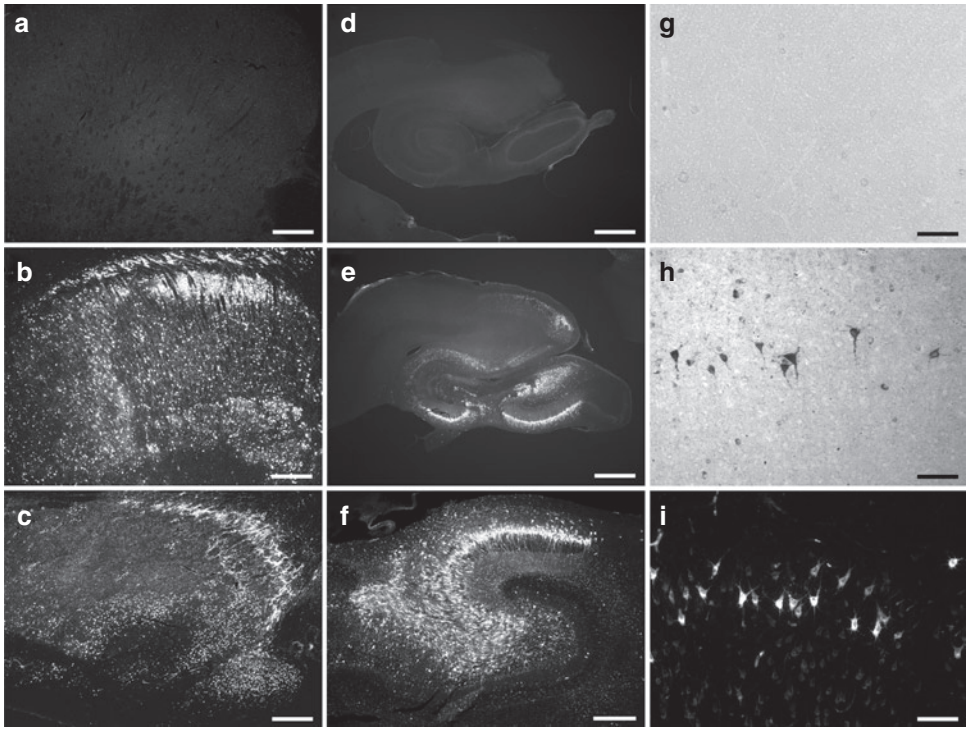

Figure 4 Subcortical injection of AAV1-hASM in NHPs. (**a**–**f**,**i**) Immunohistochemistry and (**g**,**h**) *in situ* hybridization of the (**a**,**b**) striatum, (**c**) thalamus, (**d**–**f**) hippocampus, and (**g**–**i**) entorhinal cortex in (**a**,**d**,**g**) saline-treated and (**b**,**c**,**e**,**f**,**h**,**i**) AAV1-hASM–treated monkeys. Bars: 1.0 mm (in **a**–**c**); 2.0 mm (in **d**,**e**); 0.5 mm (in **f**); 0.2 mm (in **g**–**i**). AAV, adeno-associated virus; NHP, non-human primate.

of the brain. Interestingly, a subset of brain slabs corresponding to regions outside the injection site also showed significantly elevated levels of total ASM that corroborated our histological evidence of vector-derived hASM expression in distal locations. We anticipate there to be additional low levels of vector-derived hASM in the NHP brain that would be efficacious based on the ASMKO mouse data (<0.5 ng ASM/mg tissue), but which we could not distinguish from the NHP background level. In accordance, the restoration of enzyme activity to 10–15% of normal is predicted to provide a measurable level of clinical efficacy in LSDs.[1–3]

The observed widespread pattern of hASM expression was due to several modes of vector transport in the NHP brain. The primary transduction pattern results from virions binding to cell-surface receptors within the migrating front of a given injection site. Although speculative, the transduction patterns noted in the prefrontal and occipital lobes suggest that the migrating front was aided by virions tracking along the surface of white matter tracts. The other modes of vector transport involved the escape of virions from this migrating front to establish secondary sites of transduction in distal locations. The most commonly observed mechanism of escape was axonal transport. This mechanism was most evident with DCN injections that resulted in transduction of the Purkinje cell layer, medulla oblongata, and spinal cord. Importantly, the transduction of the medulla oblongata demonstrated that regions of the CNS not readily accessible by surgery could be targeted for correction. In addition, the transduction pattern in the prefrontal and entorhinal cortices was consistent with the network of axonal connections from the striatum and hippocampus, respectively. Another mechanism of escape involved movement of the viral vector through the Virchow-Robin space, a perivascular compartment that serves as a pipeline for interstitial fluid movement through the CNS. Because all neurons are perfused by the perivascular space, it is conceivable that the viral vector became randomly distributed to distal and remote regions of the CNS by flowing through this pipeline. Finally, it is tempting to speculate that transduced cells would in turn secrete enzyme into the extracellular matrix and the protein itself be distributed by axonal transport[32] and perivascular flow[33] to establish an extensive pattern of hASM expression in the NHP brain.

LINCL is a LSD caused by mutations in *CLN2* and subsequent loss of tripeptidyl peptidase 1 (TPP1).[34] Preclinical studies showed that AAV2-TPP1 was efficacious in the LINCL mouse and could be safely delivered to the NHP.[35–37] These studies formed the basis for initiating the first CNS-directed gene therapy clinical trial for a neuronopathic LSD.[6] The significance of the LINCL experience is that TPP1 is a soluble hydrolase as is ASM, thus providing an invaluable guideline to help design clinical trials for NPA. In the first LINCL clinical trial, the $AAV2_{cu}$hCLN2 vector was injected into three cerebral cortical sites at two different depths per hemisphere for a total of 12 deposits per brain.[6,8,13] Although this multiple parenchyma injection procedure was safe and well tolerated, the report of only mild improvements in clinical scores suggested that restricting the injections to the cerebral cortex might not be sufficient to impact global storage pathology in a severely affected brain. The current study suggests that spreading the 12 deposits to subcortical and cerebellar regions might improve the overall distribution of therapeutic enzyme in the CNS in a clinical study. Other gene therapy clinical trials for neurodegenerative diseases have

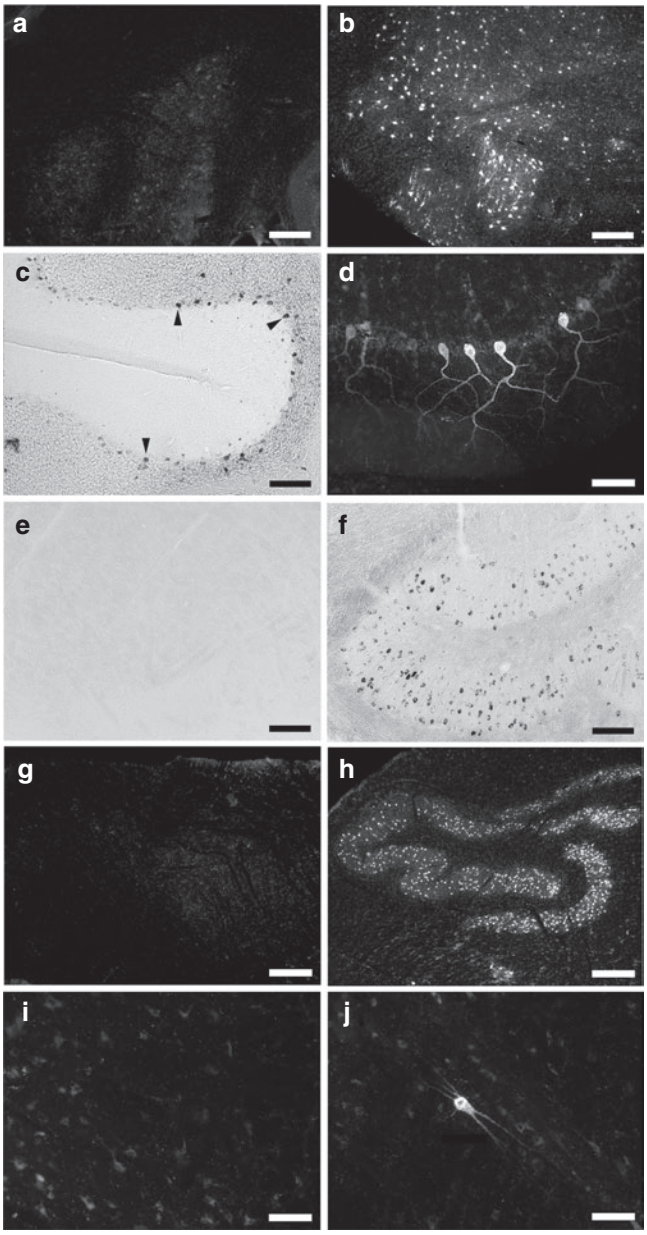

Figure 5 Cerebellar injection of AAV1-hASM in NHPs. (**a**,**b**,**d**,**g**–**j**) Immunohistochemistry and (**c**,**e**,**f**) *in situ* hybridization of the (**a**,**b**) DCN injection site, (**c**,**d**) the cerebellar cortex, (**e**–**h**) the medulla oblongata, and (**i**,**j**) the spinal cord. (**c**) The arrowheads point to examples of transduced cells (**d**) that contained classical Purkinje cell morphology in the correct laminar layer. (**f**,**h**) Clear evidence of retrograde axonal transport of AAV followed by hASM expression was observed in the medulla oblongata. (**j**) Human ASM protein was also observed in large neurons of the spinal cord. Bars: 0.2 mm (in **a**–**c**,**e**,**f**); 0.05 mm (in **d**,**i**,**j**); 0.4 mm (in **g**,**h**). AAV, adeno-associated virus; DCN, deep cerebellar nucleus; NHP, non-human primate.

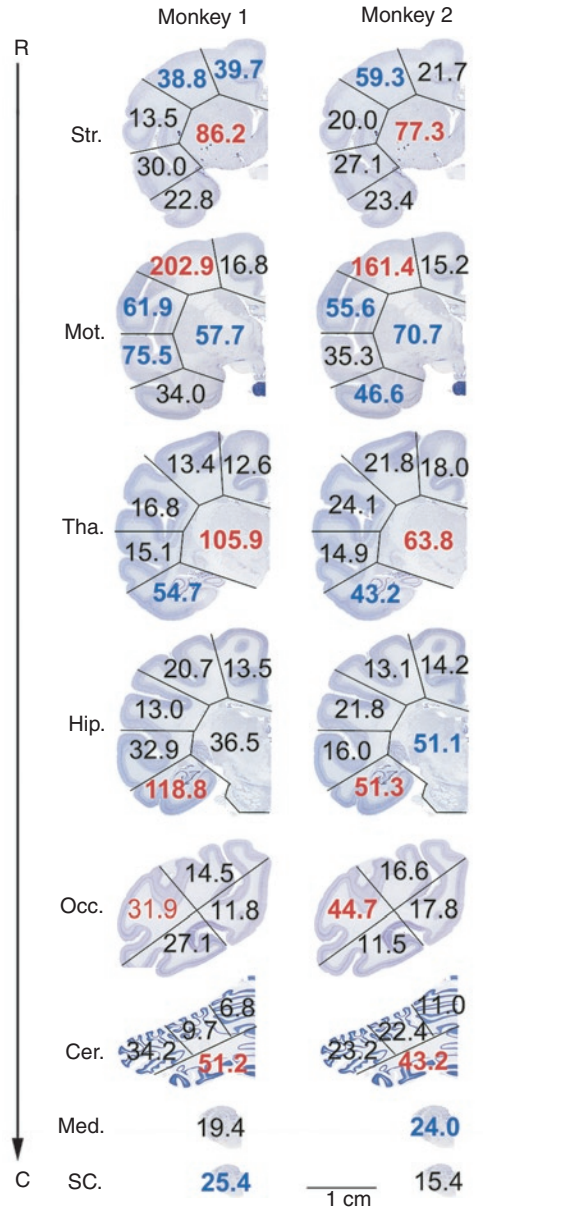

Figure 6 Summary of the total ASM levels along the rostral (R) to caudal (C) axis of the cynomolgus brain, as determined by ELISA assay. The baseline level in the saline-treated brain was 23.745 ng/mg ± 6.853 ng ASM/mg tissue (mean ± SD). Shown are the total ASM values (monkey ASM + AAV1 vector-derived hASM) in different brain slabs at the level of the injected striatum (Str.), motor cortex (Mot.), thalamus (Tha.), hippocampus (Hip.), occipital cortex (Occ.), and cerebellum (Cer.). Total ASM levels in brain slabs that contained an injection site are shown in red, which ranged from 4.0–26.1 (monkey 1) and 2.8–20.1 (monkey 2) SDs above the baseline mean. The only exception was the injected occipital cortex of monkey 1, which did not result in a significant increase in total ASM for unknown reasons. Brain slabs outside the injection sites that contained total ASM levels that were at least 2.0 SDs above the baseline mean are shown in blue. Brain slabs that were below 2.0 SDs were not significantly elevated and are shown in black. The medulla oblongata (Med.) and spinal cord (SC.) are contiguous structures that contained a low baseline level of 12.340 ± 4.904 ng ASM/mg tissue (mean ± SD) in the saline-treated monkey. DCN injections with AAV1-hASM resulted in total ASM levels that were 2.4 and 2.7 SDs above the baseline mean in the medulla oblongata of monkey 2 and the spinal cord of monkey 1, respectively. AAV, adeno-associated virus; ASM, acid sphingomyelinase; DCN, deep cerebellar nucleus.

shown that subcortical injections of AAV vectors are safe and well tolerated in humans. Specifically, the AAV2-AADC and AAV2-CERE-120 clinical trials for Parkinson's disease involved injections into the striatum,[9–11,14] the AAV2-GAD trial for Parkinson's disease involved injections into the subthalamic nucleus,[7] and the AAV2-CERE-110 trial for Alzheimer's disease involved injections into the nucleus basalis of Meynert.[12]

Although multiple convection-enhanced injections into the brain provide a conduit for widespread enzyme spread in the CNS, and that MRI guidance reduces the risk of trans-sulci piercing by the catheter, the probability of cerebral hemorrhaging will inevitably increase as the number of injection sites (tracks) increase. The potential for this adverse event could be decreased with the development of less invasive delivery strategies including intracerebroventricular or intrathecal injection. However, the literature suggests that these methods of delivery result in vector-derived enzyme expression to be restricted primarily to the periventricular regions and/or the dorsal root ganglia in neuronopathic LSD mouse models, such as for mucopolysaccharidosis III (MPS III).[38–40] These results prompted the development of a multiple parenchymal injection approach for MPS III in the Sanfilippo canine model[41] and in the upcoming clinical trial (http://www.ClinicalTrials.gov, NCT01474343). The MPS III and second LINCL upcoming trials are similar in design to the first LINCL clinical trial, except they will be utilizing an AAVrh10 serotype vector.[42] As with AAV1, AAVrh10 produced more widespread vector and enzyme distribution in the brain and improved efficacy in the LINCL mouse compared to AAV2.[43–45] These studies suggest that serotypes additional to AAV2 should be considered for the clinic, and it is the hope that AAVrh10 will improve the clinical outcome following 12 deposits into the cerebral cortex of MPS III and LINCL children.

In conclusion, AAV-mediated enzyme augmentation therapy is efficacious following intracranial injections of the viral vector into ASMKO mice. The AAV dose-response study showed that a slight decrease in SPH levels afforded by low levels of hASM was sufficient to improve the median survival of ASMKO mice. Importantly, multiple injections into the NHP brain provided widespread hASM levels that spanned from the prefrontal cortex to the brain stem and spinal cord. Significant increases in ASM levels in both injected and noninjected brain regions indicated that the topographical organization of the brain circuits and the anatomical feature of the Virchow-Robin space might be exploited to express therapeutic enzyme throughout the CNS, including regions not easily accessible by surgery. Thus, a MRI-guided combinatory cortical, subcortical, and cerebellar injection of AAV reported in the current study may serve as an alternative approach to the cortical-only injection protocols currently in use in clinical trials for neuronopathic LSDs.

MATERIAL AND METHODS

AAV vector. The AAV shuttle plasmid contained serotype-2 inverted terminal repeats and the human ASM cDNA under the transcriptional control of the 1.7 kb cytomegalovirus enhancer/chicken β-actin promoter. The shuttle plasmid was cross-packaged into serotype-1 capsids by triple plasmid co-transfection and column purification.[18] Recombinant virus (AAV1-hASM) was concentrated to a final titer of 5×10^{12} gc/ml as determined by TaqMan PCR against the bovine growth hormone polyadenylation signal sequence.

Mice and surgery. All surgical procedures were performed under protocols approved by the Institutional Animal Care and Use Committee at Genzyme. Littermates from heterozygote breeding pairs were genotyped by PCR identify wild-type and ASMKO mice.[16] On the day of surgery, dilutions of the AAV1-hASM vector were made with saline to generate injectable titers of 5.0×10^{12} gc/ml, 1.7×10^{12} gc/ml, 5.0×10^{11} gc/ml, and 1.7×10^{11} gc/ml. Eight week old ASMKO mice were anesthetized, fitted on a stereotactic frame and burr-holes were made in the skull as described.[17–19] A mounted Hamilton syringe was used to inject 4 µl of AAV1-hASM into the motor cortex (0.50 mm rostral of bregma, 1.75 mm right of midline, 1.25 mm ventral of pia), hippocampus (2.00 mm caudal of bregma, 1.75 mm right of midline, 1.75 mm ventral of pia), and DCN (6.00 mm caudal of bregma, 1.50 mm right of midline, 2.25 mm ventral of pia) of the right hemisphere, and into the striatum (0.50 mm rostral of bregma, 1.75 mm left of midline, 2.75 mm ventral of pia), pons (4.00 caudal of bregma, 1.00 left of midline, 3.50 mm ventral of pia), and DCN (6.00 mm caudal of bregma, 1.50 mm left of midline, 2.25 mm ventral of pia) of the left hemisphere for a total of 24 µl per brain. The final doses of the treated ASMKO mice were 1.2×10^{11}, 4.0×10^{10}, 1.2×10^{10} or 4.0×10^{9} gc/mouse. All treated and untreated ASMKO mice were monitored and euthanized when they reached moribund end-stage that included one or more of the following: pronounced ataxia, inability to walk in a straight line without tumbling over, inability to groom, loss of 20% body weight, or chronic dehydration. Six mice from each group were randomly selected for analysis: untreated ASMKO mice at 33, 34, 35, 36, 37, 37 weeks of age; 1.2×10^{11}-treated ASMKO mice at 36, 41, 50, 52, 52, 60 weeks of age; 4.0×10^{10}-treated ASMKO mice at 36, 38, 42, 42, 46, 52 weeks of age; 1.2×10^{10}-treated ASMKO mice at 39, 42, 42, 43, 43, 43 weeks of age; 4.0×10^{9}-treated ASMKO mice at 37, 39, 40, 41, 41, 42 weeks of age; untreated wild-type mice at 40, 50, 50, 50, 60, 60 weeks of age. Mice were perfused with phosphate-buffered saline and the brains were removed and cut into 2-mm slabs along the coronal axis to generate 4 slabs/hemisphere (see **Figure 1** for diagram). Each brain slab was flash-frozen in liquid nitrogen and stored at −80 °C until further use. Left hemisphere brain slabs were analyzed for hASM levels by an ELISA assay, and the brain slabs of the right hemisphere were analyzed for SPH levels.

Monkeys and surgery. All surgical procedures were performed under protocols approved by the Institutional Animal Care and Use Committee at the University of California San Francisco (UCSF). Male cynomolgus monkeys ($n = 3$; 2 years of age) were purchased from the California National Primate Research Center (University of California Davis, Davis, CA) and allowed to acclimate to the housing conditions at UCSF. One week before surgery, the three monkeys underwent MRI of the brain to determine the stereotactic coordinates of the injection sites.[20] On the day of surgery, the monkeys were anesthetized and fitted onto a stereotactic frame and burr-holes were made as previously described.[20] AAV1-hASM ($n = 2$) or saline ($n = 1$) was injected by convection-enhanced delivery (CED) into each of the striatum, motor cortex, thalamus, hippocampus, occipital cortex, and DCN of both hemispheres for a total of 12 injections per brain. The CED injections involved escalating rates of infusion that included 0.2 µl/minute (10 minutes), 0.5 µl/minute (10 minutes), 0.8 µl/minute (10 minutes), and 1 µl/minute (35 minutes) for the motor cortex, striatum, thalamus, and occipital cortex; and 0.2 µl/minute (10 minutes), 0.5 µl/minute (10 minutes), 0.8 µl/minute (10 minutes), and 1 µl/minute (15 minutes) for the hippocampus and DCN. The injections were done simultaneously to expedite the surgery that was well tolerated, and there were no reported adverse events in the treated monkeys during the in-life assessments by the UCSF veterinarian staff. The monkeys were transcardially perfused with phosphate-buffered saline at 5 weeks postinjection. The brain was removed and dissected into 6-cm slabs along the coronal axis, and the two hemispheres were separated from each other. The left hemisphere from each 6-cm coronal slab was further subdivided into additional pieces, flash-frozen in liquid nitrogen, and stored at −80 °C until used for ELISA. The right hemisphere from each 6-cm slab was drop-fixed in 4% paraformaldehyde for 72 hours, cryoprotected in 30% sucrose for 1 week, sectioned on a cryostat at 40 µm thickness, and stored free-floating in antifreeze solution at −20 °C. Tissue sections were processed by immunohistochemistry for vector-derived hASM protein and *in situ* hybridization for vector-derived hASM mRNA as reported.[17] The medulla oblongata and attached cervical spinal cord was also removed and the two hemispheres were separated from each other and processed in the same manner as the brain.

ASM ELISA. Brain slabs from mice and monkeys were homogenized and analyzed by ELISA as previously described.[18,19] The rabbit polyclonal anti-hASM antibody (Genzyme, Framingham, MA) does not cross-react with mouse ASM, indicating that the ELISA values generated in the ASMKO dose-response experiment were solely contributed by AAV1-hASM. In contrast, the rabbit polyclonal anti-hASM antibody does cross-react with monkey ASM, thus the ELISA values generated in the NHP biodistribution experiment represent total ASM levels (endogenous monkey ASM and AAV1 vector-derived hASM).

SPH assay. Quantification of SPH levels in tissue samples was performed as reported previously.[19] Briefly, frozen tissue samples at a concentration of 5 mg/ml were homogenized in 1:2 chloroform:methanol. Clarified lysates were back-extracted with water, dried down, and stored frozen. The amount of SPH in tissue extracts was quantified using the Amplex Red sphingomyelinase kit (Molecular Probes, Eugene, OR). Purified sphingomyelin C18 (Matreya, Pleasant Gap, PA) was used as the standard. SPH levels were normalized to the wet-weights of the tissues.

Statistics. All statistical analysis were performed with GraphPad Prism v5.0a (GraphPad Software, San Diego, CA). Values that were at least $P < 0.05$ were considered significant. Statistical analyses of the SPH levels and the Kalpan–Meier survival curve in the AAV1-hASM dose-response experiment was performed by one-way analysis of variance and Bonferroni multiple post hoc comparisons, and the log-rank test equivalent to the Mantel–Haenszel test, respectively. To determine whether there were significant increases in total ASM levels after AAV1-hASM treatment in NHPs, ELISA values of the corresponding brain slabs (not including the medulla) from the saline-treated monkey produced a normality of distribution and a baseline level of 23.745 ± 6.853 ng ASM/mg tissue (mean ± SD). The ELISA value from each individual brain slab in the AAV1-hASM–treated monkeys was then compared to this baseline level using a two-tailed P value analysis of the calculated Z-scores (SDs). Brain slabs with total ASM levels that contained at minimum Z-score (SDs) of 2.0 above the baseline mean of the saline-treated monkey were considered statistically significant. The medulla oblongata and spinal cord from the saline-treated monkey had a significantly less baseline level of 12.340 ± 4.904 ng ASM/mg tissue (mean ± SD) compared to the brain baseline level, as determined by an unpaired two-tailed Student's t-test ($P = 0.0020$). Appropriately, the medulla oblongata and spinal cord slabs of the AAV1-hASM–treated monkeys were thus compared to this lower baseline using the same two-tailed/Z-score analysis.

ACKNOWLEDGMENTS

We thank Robin Zeigler and Joseph Foley for assistance with the SPH assays, Catherine O'Riordan and the Genzyme Vector Core for virus production, and Philip Pivirotto for assistance with NHP surgery. J.B., K.M.A., J.M., J.C.D., M.A.C.-S., S.H.C., L.S.S., and M.A.P. are paid employees of Genzyme, and E.H.S. and K.S.B. are paid consultants of Genzyme. The other authors declared no conflict of interest.

REFERENCES

1. Schultz, ML, Tecedor, L, Chang, M and Davidson, BL (2011). Clarifying lysosomal storage diseases. *Trends Neurosci* **34**: 401–410.
2. Sands, MS and Haskins, ME (2008). CNS-directed gene therapy for lysosomal storage diseases. *Acta Paediatr Suppl* **97**: 22–27.
3. Sands, MS and Davidson, BL (2006). Gene therapy for lysosomal storage diseases. *Mol Ther* **13**: 839–849.
4. Gray, SJ, Matagne, V, Bachaboina, L, Yadav, S, Ojeda, SR and Samulski, RJ (2011). Preclinical differences of intravascular AAV9 delivery to neurons and glia: a comparative study of adult mice and nonhuman primates. *Mol Ther* **19**: 1058–1069.
5. Janson, C, McPhee, S, Bilaniuk, L, Haselgrove, J, Testaiuti, M, Freese, A *et al.* (2002). Clinical protocol: gene therapy of Canavan disease: AAV-2 vector for neurosurgical delivery of aspartoacylase gene (ASPA) to the human brain. *Hum Gene Ther* **13**: 1391–1412.
6. Crystal, RG, Sondhi, D, Hackett, NR, Kaminsky, SM, Worgall, S, Stieg, P *et al.* (2004). Clinical protocol: administration of a replication-deficient adeno-associated virus gene transfer vector expressing the human CLN2 cDNA to the brain of children with late infantile neuronal ceroid lipofuscinosis. *Hum Gene Ther* **15**: 1131–1154.
7. Kaplitt, MG, Feigin, A, Tang, C, Fitzsimons, HL, Mattis, P, Lawlor, PA *et al.* (2007). Safety and tolerability of gene therapy with an adeno-associated virus (AAV) borne GAD gene for Parkinson's disease: an open label, phase I trial. *Lancet* **369**: 2097–2105.
8. Worgall, S, Sondhi, D, Hackett, NR, Kosofsky, B, Kekatpure, MV, Neyzi, N *et al.* (2008). Treatment of late infantile neuronal ceroid lipofuscinosis by CNS administration of a serotype 2 adeno-associated virus expressing CLN2 cDNA. *Hum Gene Ther* **19**: 463–474.
9. Marks, WJ Jr, Ostrem, JL, Verhagen, L, Starr, PA, Larson, PS, Bakay, RA *et al.* (2008). Safety and tolerability of intraputaminal delivery of CERE-120 (adeno-associated virus serotype 2-neurturin) to patients with idiopathic Parkinson's disease: an open-label, phase I trial. *Lancet Neurol* **7**: 400–408.
10. Eberling, JL, Jagust, WJ, Christine, CW, Starr, P, Larson, P, Bankiewicz, KS *et al.* (2008). Results from a phase I safety trial of hAADC gene therapy for Parkinson disease. *Neurology* **70**: 1980–1983.
11. Christine, CW, Starr, PA, Larson, PS, Eberling, JL, Jagust, WJ, Hawkins, RA *et al.* (2009). Safety and tolerability of putaminal AADC gene therapy for Parkinson disease. *Neurology* **73**: 1662–1669.
12. Mandel, RJ (2010). CERE-110, an adeno-associated virus-based gene delivery vector expressing human nerve growth factor for the treatment of Alzheimer's disease. *Curr Opin Mol Ther* **12**: 240–247.
13. Souweidane, MM, Fraser, JF, Arkin, LM, Sondhi, D, Hackett, NR, Kaminsky, SM *et al.* (2010). Gene therapy for late infantile neuronal ceroid lipofuscinosis: neurosurgical considerations. *J Neurosurg Pediatr* **6**: 115–122.
14. Muramatsu, S, Fujimoto, K, Kato, S, Mizukami, H, Asari, S, Ikeguchi, K *et al.* (2010). A phase I study of aromatic L-amino acid decarboxylase gene therapy for Parkinson's disease. *Mol Ther* **18**: 1731–1735.
15. Schuchman, EH and Desnick, RJ (2001). Niemann-Pick disease Types A and B: acid sphingomyelinase deficiencies. In: Scriver, CR, Beaudet, AL, Sly, WS and Valle, D (eds). *The Metabolic and Molecular Basis of Inherited Disease*, 8th edn. McGraw-Hill: New York. pp. 3589–3610.
16. Horinouchi, K, Erlich, S, Perl, DP, Ferlinz, K, Bisgaier, CL, Sandhoff, K *et al.* (1995). Acid sphingomyelinase deficient mice: a model of types A and B Niemann-Pick disease. *Nat Genet* **10**: 288–293.
17. Passini, MA, Macauley, SL, Huff, MR, Taksir, TV, Bu, J, Wu, IH *et al.* (2005). AAV vector-mediated correction of brain pathology in a mouse model of Niemann-Pick A disease. *Mol Ther* **11**: 754–762.
18. Dodge, JC, Clarke, J, Song, A, Bu, J, Yang, W, Taksir, TV *et al.* (2005). Gene transfer of human acid sphingomyelinase corrects neuropathology and motor deficits in a mouse model of Niemann-Pick type A disease. *Proc Natl Acad Sci USA* **102**: 17822–17827.
19. Passini, MA, Bu, J, Fidler, JA, Ziegler, RJ, Foley, JW, Dodge, JC *et al.* (2007). Combination brain and systemic injections of AAV provides maximal functional and survival benefits in Niemann-Pick mice. *Proc Natl Acad Sci USA* **104**: 9505–9510.
20. Salegio, EA, Kells, AP, Richardson, RM, Hadaczek, P, Forsayeth, J, Bringas, J *et al.* (2010). Magnetic resonance imaging-guided delivery of adeno-associated virus type 2 to the primate brain for the treatment of lysosomal storage disorders. *Hum Gene Ther* **21**: 1093–1103.
21. Wang, C, Wang, CM, Clark, KR and Sferra, TJ (2003). Recombinant AAV serotype 1 transduction efficiency and tropism in the murine brain. *Gene Ther* **10**: 1528–1534.
22. Passini, MA, Watson, DJ, Vite, CH, Landsburg, DJ, Feigenbaum, AL and Wolfe, JH (2003). Intraventricular brain injection of adeno-associated virus type 1 (AAV1) in neonatal mice results in complementary patterns of neuronal transduction to AAV2 and total long-term correction of storage lesions in the brains of beta-glucuronidase-deficient mice. *J Virol* **77**: 7034–7040.
23. Burger, C, Gorbatyuk, OS, Velardo, MJ, Peden, CS, Williams, P, Zolotukhin, S *et al.* (2004). Recombinant AAV viral vectors pseudotyped with viral capsids from serotypes 1, 2, and 5 display differential efficiency and cell tropism after delivery to different regions of the central nervous system. *Mol Ther* **10**: 302–317.
24. Burger, C, Nash, K and Mandel, RJ (2005). Recombinant adeno-associated viral vectors in the nervous system. *Hum Gene Ther* **16**: 781–791.
25. Vite, CH, McGowan, JC, Niogi, SN, Passini, MA, Drobatz, KJ, Haskins, ME *et al.* (2005). Effective gene therapy for an inherited CNS disease in a large animal model. *Ann Neurol* **57**: 355–364.
26. Klein, RL, Dayton, RD, Leidenheimer, NJ, Jansen, K, Golde, TE and Zweig, RM (2006). Efficient neuronal gene transfer with AAV8 leads to neurotoxic levels of tau or green fluorescent proteins. *Mol Ther* **13**: 517–527.
27. Hadaczek, P, Forsayeth, J, Mirek, H, Munson, K, Bringas, J, Pivirotto, P *et al.* (2009). Transduction of non-human primate brain with adeno-associated virus serotype 1: vector trafficking and immune response. *Hum Gene Ther* **20**: 225–237.
28. Ciron, C, Cressant, A, Roux, F, Raoul, S, Cherel, Y, Hantraye, P *et al.* (2009). Human alpha-iduronidase gene transfer mediated by adeno-associated virus types 1, 2, and 5 in the brain of nonhuman primates: vector diffusion and bio-distribution. *Hum Gene Ther* **20**: 350–360.
29. Hutson, TH, Verhaagen, J, Yáñez-Muñoz, RJ and Moon, LD (2012). Corticospinal tract transduction: a comparison of seven adeno-associated viral vector serotypes and a non-integrating lentiviral vector. *Gene Ther* **19**: 49–60.
30. Hadaczek, P, Yamashita, Y, Mirek, H, Tamas, L, Bohn, MC, Noble, C *et al.* (2006). The "perivascular pump" driven by arterial pulsation is a powerful mechanism for the distribution of therapeutic molecules within the brain. *Mol Ther* **14**: 69–78.
31. Kells, AP, Hadaczek, P, Yin, D, Bringas, J, Varenika, V, Forsayeth, J *et al.* (2009). Efficient gene therapy-based method for the delivery of therapeutics to primate cortex. *Proc Natl Acad Sci USA* **106**: 2407–2411.
32. Passini, MA, Lee, EB, Heuer, GG and Wolfe, JH (2002). Distribution of a lysosomal enzyme in the adult brain by axonal transport and by cells of the rostral migratory stream. *J Neurosci* **22**: 6437–6446.
33. Jolly, RD, Marshall, NR, Perrott, MR, Dittmer, KE, Hemsley, KM and Beard, H (2011). Intracisternal enzyme replacement therapy in lysosomal storage diseases: routes of absorption into brain. *Neuropathol Appl Neurobiol* **37**: 414–422.

34. Sleat, DE, Donnelly, RJ, Lackland, H, Liu, CG, Sohar, I, Pullarkat, RK *et al.* (1997). Association of mutations in a lysosomal protein with classical late-infantile neuronal ceroid lipofuscinosis. *Science* **277**: 1802–1805.
35. Sondhi, D, Peterson, DA, Giannaris, EL, Sanders, CT, Mendez, BS, De, B *et al.* (2005). AAV2-mediated CLN2 gene transfer to rodent and non-human primate brain results in long-term TPP-I expression compatible with therapy for LINCL. *Gene Ther* **12**: 1618–1632.
36. Hackett, NR, Redmond, DE, Sondhi, D, Giannaris, EL, Vassallo, E, Stratton, J *et al.* (2005). Safety of direct administration of AAV2CUhCLN2, a candidate treatment for the central nervous system manifestations of late infantile neuronal ceroid lipofuscinosis, to the brain of rats and nonhuman primates. *Hum Gene Ther* **16**: 1484–1503.
37. Passini, MA, Dodge, JC, Bu, J, Yang, W, Zhao, Q, Sondhi, D *et al.* (2006). Intracranial delivery of CLN2 reduces brain pathology in a mouse model of classical late infantile neuronal ceroid lipofuscinosis. *J Neurosci* **26**: 1334–1342.
38. Watson, G, Bastacky, J, Belichenko, P, Buddhikot, M, Jungles, S, Vellard, M *et al.* (2006). Intrathecal administration of AAV vectors for the treatment of lysosomal storage in the brains of MPS I mice. *Gene Ther* **13**: 917–925.
39. Liu, G, Martins, I, Wemmie, JA, Chiorini, JA and Davidson, BL (2005). Functional correction of CNS phenotypes of CNS phenotypes in a lysosomal storage disease model using adeno-associated virus type 4 vectors. *J Neurosci* **25**: 9321–9327.
40. Fu, H, Kang, L, Jennings, JS, Moy, SS, Perez, A, Dirosario, J *et al.* (2007). Significantly increased lifespan and improved behavioral performances by rAAV gene delivery in adult mucopolysaccharidosis IIIB mice. *Gene Ther* **14**: 1065–1077.
41. Ellinwood, NM, Ausseil, J, Desmaris, N, Bigou, S, Liu, S, Jens, JK *et al.* (2011). Safe, efficient, and reproducible gene therapy of the brain in the dog models of Sanfilippo and Hurler syndromes. *Mol Ther* **19**: 251–259.
42. de Melo-Martín, I, Sondhi, D and Crystal, RG (2011). When ethics constrains clinical research: trial design of control arms in "greater than minimal risk" pediatric trials. *Hum Gene Ther* **22**: 1121–1127.
43. Cabrera-Salazar, MA, Roskelley, EM, Bu, J, Hodges, BL, Yew, N, Dodge, JC *et al.* (2007). Timing of therapeutic intervention determines functional and survival outcomes in a mouse model of late infantile batten disease. *Mol Ther* **15**: 1782–1788.
44. Sondhi, D, Hackett, NR, Peterson, DA, Stratton, J, Baad, M, Travis, KM *et al.* (2007). Enhanced survival of the LINCL mouse following CLN2 gene transfer using the rh.10 rhesus macaque-derived adeno-associated virus vector. *Mol Ther* **15**: 481–491.
45. Sondhi, D, Peterson, DA, Edelstein, AM, del Fierro, K, Hackett, NR and Crystal, RG (2008). Survival advantage of neonatal CNS gene transfer for late infantile neuronal ceroid lipofuscinosis. *Exp Neurol* **213**: 18–27.